C: Energy Conversion and Storage; Energy and Charge Transport

Microstructural Modeling of Composite Cathodes for All-Solid-State Batteries

Anja Bielefeld, Dominik A. Weber, and Jürgen Janek

J. Phys. Chem. C, **Just Accepted Manuscript** • DOI: 10.1021/acs.jpcc.8b11043 • Publication Date (Web): 31 Dec 2018

Microstructural Modeling of Composite Cathodes for All-Solid-State Batteries

Anja Bielefeld,[*,†,‡] Dominik A. Weber,[‡] and Jürgen Janek[*,†,¶]

†*Physikalisch-Chemisches Institut, Justus-Liebig-Universität, 35392 Giessen, Germany*

‡*Volkswagen AG, Group Research, 38436 Wolfsburg, Germany*

¶*Center of Materials Research (LaMa), Justus-Liebig-Universität, 35392 Giessen, Germany*

E-mail: anja.bielefeld@volkswagen.de; juergen.janek@phys.chemie.uni-giessen.de

Abstract

When it comes to energy density, all-solid-state batteries are seen as a promising technology for next-generation electrochemical storage devices. Nevertheless, the performance of all-solid-state cells is still very limited. The reasons are manifold, with insufficient ionic and electronic percolation within the composite cathode being a crucial one. In this work, we investigate percolation characteristics by three-dimensional microstructural modeling with the aim to define and understand boundary conditions for well-percolating networks. Utilizing spherical active material particles together with convex polyhedra as solid electrolyte, ionic and electronic conduction clusters are determined and analyzed by means of percolation theory for varying macroscopic parameters, such as composition, porosity, particle size and electrode thickness. Small active material particles turn out to enhance effective electronic conductivity, offering high surface areas and thus more possibilities to connect particles, while porosity crucially effects ionic and electronic conduction capabilities. An impact of electrode thickness on the effective electronic conductivity is observed exclusively in thin electrodes, where percolation effects are suppressed implying favorable electrode properties. From microstructural modeling, ideal compositions are derived and guidelines for electrode design are developed at a given porosity and particle size of active material and solid electrolyte.

Introduction

Conventional lithium-ion batteries are expected to approach their physical limits in energy density and fast charging anytime soon[1,2], leaving all-solid-state batteries (ASSBs) as promising candidates to promote battery technology even further: The advancement of higher energy and power densities is driven by the idea to enable lithium-metal anodes using a dense and thin, but dendrite-safe, solid electrolyte (SE) separator[3]. As bulk polarization inside such a SE can practically be excluded due to sole conduction of lithium ions (single ion conductors; transference number very close to one), ASSBs may also pave the way towards

higher current densities and fast charging[4], which is an important feature for future mobility concepts.

Despite promising sulfide-based high power cells demonstrating stable cycling at a rate of 18 C at 100 °C[5], up to date, the performance of ASSBs has been very limited in most studies[6]. The reasons are miscellaneous and different mutually non-exclusive explanations can be drawn. Performance strongly depends on material properties (elastic, (electro-)chemical and morphological), the compatibility of the cell components, and on the cell design. For once, contact loss throughout the composite cathode occurs due to volume change of the active material during cycling, as was exemplarily shown for nickel-rich $LiNi_{0.8}Co_{0.1}Mn_{0.1}O_2$ (NCM-811) and the sulfide-based solid electrolyte β-Li_3PS_4 (LPS)[7]. Moreover, the formation of a space charge layer at the interface between solid electrolyte and cathode[8], dendrite formation[9] (or interfacial defect propagation along Griffith flaws[10]) and limitations in ionic and/or electronic conduction within the cathode[11,12] are reported.

In conventional liquid electrolyte systems as well as in ASSBs, electrodes have to be designed with regard to performance featuring high capacity, power and cycling stability. These goals are achieved by providing (fast) ionic and electronic conduction pathways for charge transport, high active interface areas between electrolyte and active material (AM) for the intercalation to occur and sufficient utilization of active material. Contrary to conventional battery cells, the rigid solid electrolyte does not necessarily adhere well to the surface of the active material. This has to be taken into consideration already in the process of cathode manufacturing. The impact of electrode design on the performance of ASSBs comprising shape and size (distribution) of active material and solid electrolyte, porosity and composition as well as electrode thickness, is an important aspect yet to be investigated in depth for ASSBs.

To date, studies on the role of composition and particle size have been conducted and limitations for ionic as well as for electronic transport have been reported: On the one hand, a severe drop of electronic conductivity has been observed upon the increase of AM particle size

(up to 20 µm), using carbon-free electrodes that consist of nickel-rich NCM-622 and the thiophosphate electrolyte LPS, indicating that small AM particles enhance cell performance[13]. Similarly, the effective electronic conductivity in NCM-523 and Li_2S-P_2S_5 composites happens to be affected by the composition, indicating that a high AM/SE volume ratio enhances effective electronic conductivity, while it goes along with a decrease in effective ionic conductivity throughout the composite[14]. On the other hand, studies on the effect of electrode composition show that high mass loading of up to 85 wt-% AM leads to lower capacity and weak rate capability in NCM-622/Argyrodite/Super C65/Nitrile Butadiene Rubber (NBR) composite cathodes. The polymer binder and the small fraction of SE are considered as key reasons for the poor effective ionic conductivity[11]. More evidence for limitation in the ionic conduction at high mass loading of AM is provided by cycling and rate tests of electrodes, consisting of $LiCoO_2$ (LCO) and $Li_{10}GeP_2S_{12}$ (LGPS) at varying fractions[12], as well as for composites of $Li_{3x}La_{2/3-x}TiO_3$ (LLTO)-coated LCO and glass-ceramic LPS with Super P carbon[15]. Similarly, the porosity has been evidenced to have significant impact on the effective ionic conductivity, and therefore on tortuosity in LCO and Li_2S-P_2S_5-LiI composite electrodes, analyzed by electrochemical impedance spectroscopy and FIB-SEM reconstruction coupled with numerical simulations[16]. Moreover, thick composite cathodes of up to 600 µm have successfully been prepared and operated at room temperature using LPS and LGPS with LCO active material[17], indicating that solid electrolytes with a transference number close to unity may enable the usage of thick high energy cathodes, while conventional liquid electrolytes tend to build up concentration gradients of the conducting salt, limiting ionic transport at high C rates[1,18].

Even though the above-mentioned studies give indications upon composite electrode design, a holistic approach considering porosity, active material particle size and size distribution, as well as composition and electrode thickness as parameters of interest, has not been reported, both experimentally as well as theoretically or from a modeling perspective. In this work, we analyze ionic and electronic percolation, the utilization of active material and the

resulting active interface area in an expedient number of predefined composite cathodes by microstructural modeling.

We give a short introduction on percolation theory and explain its application to microstructural modeling of composite electrodes, as well as the layout and construction of the microstructure itself. The study on the influence of AM particle size, composition, porosity and electrode thickness allows us to predict and specify optimal conditions for high-performance composite electrodes and to understand the influence of design parameters in order to provide useful guidelines for electrode composition.

Methods

In their study on microstructural connectivity, Lagadec et al.[19] conclude that all electrochemical systems can be seen as interwoven electronic and ionic networks, which have to be balanced at all length scales, providing pathways for charge transport. Accordingly, the idea of our work is to use percolation theory to model the network of ionic and electronic conduction throughout the composite cathode of ASSBs.

Percolation Theory

Percolation theory is used for the description of critical phenomena and phase transition modeling in probability theory and originates from the analysis of percolation of fluids through a (random) porous structure[20,21].

A simulation network with occupied or non-occupied sites is created and their connectivity is examined. Identification of connected clusters is carried out starting at one chosen boundary, checking whether neighboring sites of occupied sites are occupied, as well. If so, these sites are added to the cluster. This routine continues through the whole structure, using the Hoshen-Kopelman algorithm[22]. Clusters that reach throughout the whole structure and connect both boundaries, are called percolating clusters. As a result, occupied/unoccupied

sites and, if present, occupied sites that belong to the percolating cluster, can be discerned. Apart from the existence of percolation itself, the connectivity of the percolation cluster is an interesting characteristic.

To investigate percolation phase changes, order parameters are analyzed. These parameters are also known from theory of phase transformations and exhibit sudden value changes at the percolation threshold p_c, which is defined as the critical occupation probability at which percolation is first observed and the phase transition (non-percolating to percolating) occurs. The regions below and above the critical probability are referred to as the subcritical phase ($p < p_c$) and the supercritical phase ($p > p_c$), respectively[21]. Just above the percolation threshold, percolation law predicts the order parameter to obey a power law

$$\Theta \propto (p - p_c)^{\beta}, \tag{1}$$

where Θ is the order parameter, β is the critical exponent as introduced by Grimmett[21] and p refers to the occupation probability in the critical region above and close to the threshold. In finite systems, the phase transition observed by the order parameter is expected to be smeared over an interval due to statistical variation. Only infinite systems incorporate a well-defined and discrete percolation threshold.

In ASSB electrodes, the application of percolation theory and the identification of conduction clusters may allow to estimate the effective ionic and electronic conductivity close to the percolation threshold for similar microstructures. Apart from the percolation law, the threshold itself is of interest, since the achievement of high performance in ASSB cells requires both, ionic and electronic conduction throughout the cathode (and anode) and during the whole cell lifetime[11].

Microstructural Modeling

Targeting a significant study design, the aim is to generate microstructures that are as simple as possible, while being representative for realistic composite cathodes at the same time. In general, composite cathodes for ASSBs consist of five components: Active material, solid electrolyte, conductive agent, binder and pore volume (e.g. Nam et al.[11]). For the current microstructural percolation study, the influence of binder and conductive agent are left aside, similar to the experimental analysis performed by Strauss et al.[13], but could in principle be added to such a microstructure model. A practical reason to consider renunciation of carbon black is that carbon additives have shown degradation reactions in contact with thiophosphate electrolytes during cycling[7,23,24]. Apart, cathode active material coatings play an important role for thiophosphate solid electrolytes, preventing electrochemical reactions of active material and solid electrolyte, as well as suppressing highly resistive lithium-ion-deficient layers at the interface[25]. Different coatings on cathode active material, such as partially-crystallized $Li_{56}Nb_{22}Ta_{22}$-oxide[26], $Li_4Ti_5O_{12}$[25], $LiNbO_3$[27,28] and Li_2O-ZrO_2[29] have shown to improve cell performance. Concerning the percolation study, active material coatings are considered to have negligible impact on percolation networks and therefore on effective conductivities due to their nanoscale thickness and sufficient charge transport properties[26].

On this basis, the electronic conduction through the cathode is exclusively provided by connected active material particles, since the solid electrolyte is a single ion conductor with negligible electronic conductivity. With the percolation study carried out on a three-dimensional microstructure, the outer boundary conditions for sufficiently well-connected particles are to be found.

The microstructural modeling approach in GeoDict®,[30] is schematically shown in Figure 1, assuming a two-component cathode consisting of two sub-models, one for the solid electrolyte (e.g. lithium thiophosphate electrolyte, LPS) and one for the active material particles (e.g. NCM-811). Both sub-structures are generated separately and merged afterwards. The active

material is modeled by spherical particles with a uniform particle size distribution and no overlap. Even though leading to oversimplification, a uniform particle size is chosen in this work to isolate the influence of particle size itself from possibly biasing distribution settings. As an example, a Gaussian distribution with a given width and bi- or trimodal distributions introduce more input parameters whose influence on percolation is to be analyzed in future studies. In sub-model-creation, the AM particles are distributed randomly throughout the microstructure, so that none of the modeled microstructures looks like the other. After creation of all particles up to a given solid volume fraction, the overlap is removed by allowing overlapping particles (one by one) to shift within a given distance. If this process does not eliminate the overlap, it is repeated ten times for the particle. Doing so, the overlap could be minimized to around 10^{-5} vol% in most cases. The overlap removal gets difficult at elevated solid volume fractions, since the particles are densely packed. In case of the highest AM volume fractions (around 65 vol%), the overlap reaches values of up to 1 %, which is explicable by the proximity to the geometrical limit for dense packing of equally sized spheres at

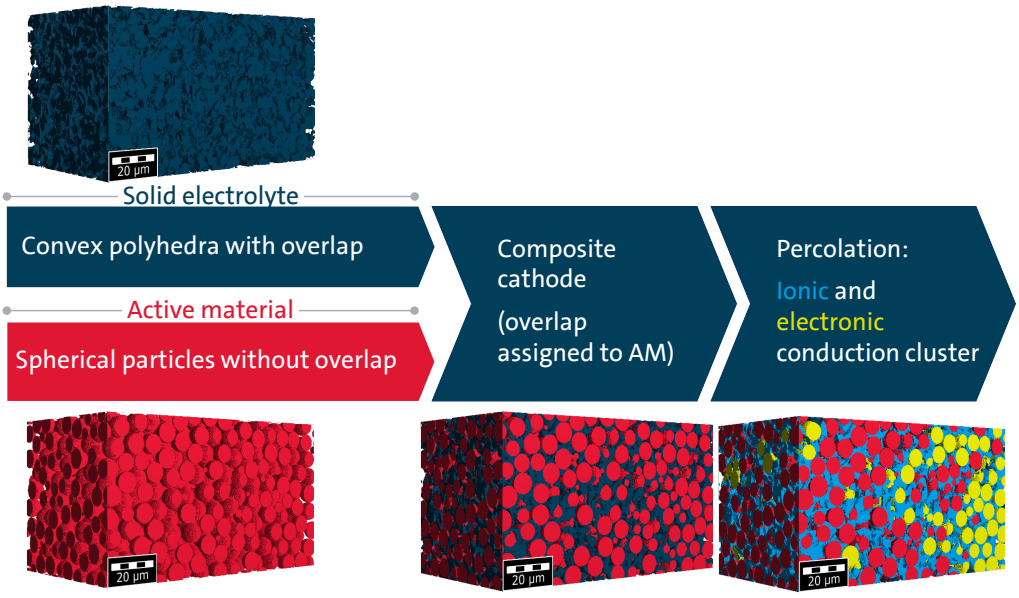

Figure 1: Microstructural modeling of composite cathodes in GeoDict®,[30] featuring spherical active material particles (red), convex polyhedra as solid electrolyte (dark blue) and ionic (light blue) as well as electronic (yellow) conduction clusters.

74 %[31]. Introduction of non-uniform particle distributions would shift this limits towards higher packing densities.

The solid electrolyte is incorporated as convex polyhedra with overlap, which is a reasonable assumption for thiophosphate electrolytes, due to their relatively low Young's modulus of ~ 25 GPa[32–34] and good ductility. The SE particle size corresponds to the enclosing sphere diameter. The marriage of the active material and electrolyte sub-structures is carried out by assigning the overlap to the active material particles for them to remain spherical. This results in a loss of solid electrolyte within the composite, which has to be compensated *a priori* by generating a denser electrolyte sub-structure.

The volume which is neither filled with active material nor with solid electrolyte is the pore volume V_{pore}. The fraction of pores, with respect to the microstructure volume V_{total}, is referred to as the porosity

$$\phi = \frac{V_{\mathrm{pore}}}{V_{\mathrm{total}}} \tag{2}$$

or, expressed in terms of volume filled by active material V_{AM} and solid electrolyte V_{SE},

$$\phi = 1 - \frac{V_{\mathrm{AM}} + V_{\mathrm{SE}}}{V_{\mathrm{total}}}. \tag{3}$$

Calculating the volume fractions of active material and solid electrolyte for microstructure construction, one has to distinguish volume fractions with respect to the total structure volume with superscript V, taking porous volume into account, from volume fractions with respect to the solid phase only. These are referred to by superscript S and can directly be found in the composition indication. At given composition and porosity, the fraction of active material in the whole volume $g^{\mathrm{V}}_{\mathrm{AM}}$, including porosity, can then be calculated as

$$g^{\mathrm{V}}_{\mathrm{AM}} = (1 - g^{\mathrm{S}}_{\mathrm{SE}})(1 - \phi), \tag{4}$$

while the electrolyte fraction is adjusted to

$$g_{\mathrm{SE}}^{\mathrm{V}} = \frac{(1-\phi)}{(1-\phi) + \frac{\phi}{g_{\mathrm{SE}}^{\mathrm{S}}}}. \tag{5}$$

Equation 5 calculates the solid volume fraction that has to be occupied by electrolyte in the SE-sub-structure. Hence, at the point of SE-sub-structure generation, active material is not yet present, but will later (in the marriage) consume parts of the SE-sub-structure, so that finally the desired composition and/or porosity is achieved.

Combining the microstructure with the material properties, the ionic and electronic conduction clusters can be identified. Due to the fact that desirable solid electrolytes are purely ion conductors and do not provide any electronic conduction paths, they only contribute to the ionic conduction cluster. The active material is assumed to have negligible ionic conductivity compared to the electrolyte (about five to six orders of magnitude lower[35]), and is therefore solely assigned to the electronic conduction cluster.

These clusters are computed by checking for connected components, starting from one boundary plane, which is fully connected to either the current collector in the electronic case or to the solid electrolyte separator in the ionic conduction case. In Figure 1, these conduction clusters are shown in yellow (electronic) and light blue (ionic), respectively.

In order to model thick electrodes that reflect the demands of future solid-state technology, a relatively large electrode thickness of 140 µm is chosen at a resolution of 200 nm, which is reasonable to model particle sizes down to 3 µm. The general microstructural modeling input parameters can be found in Table 1.

Table 1: General microstructural modeling input parameters.

Parameter	Value
Microstructure dimensions	(80 x 80 x 140) μm^3
Resolution	0.2 μm/voxel
Shape of active material	spherical
Particle size of active material	$\{3, 4, 5, 6, 7, 8, 9, 10, 15\}$ μm
Particle size distribution of active material	uniform
Shape of solid electrolyte	convex polyhedra
Particle size of solid electrolyte	3 μm

Results and discussion

For the evaluation of ionic and electronic percolation in composite cathode microstructures, different microstructural parameters, reflecting the percolation properties, can be studied. A comparison of the volume fraction of both solid components allows to compute the utilization level, which for example, indicates the ratio of the volume of active material that is assigned to the conduction cluster and the volume of active material that is not part of the cluster and therefore lost in terms of battery performance. The utilization level can be expressed as

$$\theta_\nu = \frac{V_\mathrm{c}}{V_\nu}, \tag{6}$$

where subscript c refers to the cluster, either ionic or electronic, and ν to the solid component, either active material or solid electrolyte.

Other than that, the surface area A_spec, specific to the structure volume and measured in m^2/m^3, can be computed for the ionic or electronic cluster separately or as the active interface area between the ionic and the electronic conduction cluster $A_\mathrm{spec,a}$. In terms of cell performance, the active interface area is the area available for intercalation of lithium-ions into the active material and should be maximized to assure high energy and power density. Apart from ionic intercalation, electronic conduction has to be assured as well: The active material is assumed to be the only electronically conducting material in the modeled composite, so electrons have to be transferred from one AM particle to the other. In the

current study, due to the percolation theory approach, conduction networks are analyzed. These do not take into account possible resistances occurring at particle-particle interfaces and constriction resistances which reflect the fact, that electric contacts have to be regarded as a large number of interacting mircocontacts[36].

Electronic Conduction

We will first consider electronic conduction clusters only, varying the fraction of active material in the microstructures. Furthermore, the impact of particle size is examined by generation of microstructures with particle sizes between 3 and 15 µm, demonstrating the applicability of the power law of percolation theory (see Equation 1). As an example, Figure 2 presents three microstructures and their electronic conduction clusters, all at an AM fraction of 55 vol%. From left to right, the AM particle sizes grow from 5 µm to 15 µm. The electronic cluster percolates well for the small particles, whereas medium-sized particles involve a smaller utilization level of active material and the large particles do not feature a percolating cluster, at all.

Computation of utilization level and specific surface area for different active material fractions shows a percolation transition for 5 µm-sized particles (Figure 3). According to their definitions, both properties obey the same curve progression: When more active material is used and the utilization level rises, the surface area of the electronic cluster increases. At this point, the main difference is that the utilization level is a normalized property, whereas

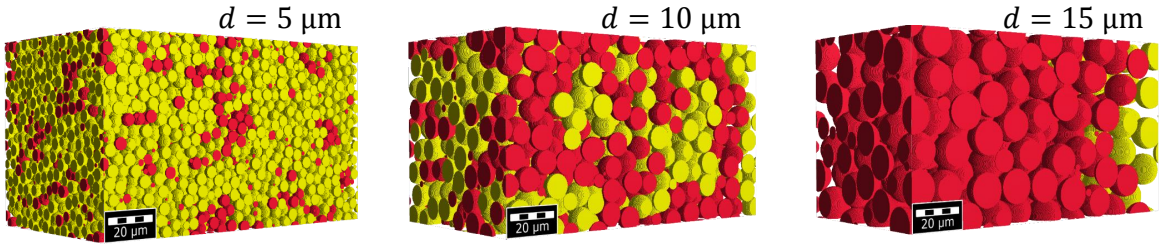

Figure 2: Exemplary active material microstructures at 55 vol% fraction for $\{5, 10, 15\}$ µm particle diameter and respective electronic clusters (yellow). Non-connected particles are shown in red.

the change for the absolute values of the surface area depends on particle size. For active material fractions below 48 vol%, both values are very low, indicating that the particles are poorly connected and the conduction cluster does not reach far into the composite microstructure. The small perturbation at 45 vol% is due to the fact that these data points are based on one particle arrangement for each volume fraction. In the transition region between 48 and 52 vol%, ten random microstructures were computed for each fraction to avoid too high uncertainties and to attain a statistically more profound conclusion. The uncertainties arise due to statistical fluctuations from particle arrangement to particle arrangement. Depending on the random packing, some arrangements percolate with AM utilization levels around 70 %, while others, at the same AM fraction, do not percolate and therefore exhibit utilization levels around 30 %. In this region, the utilization level steeply increases, indicating that the transition takes place, while above 52 vol% AM fraction, the gradient diminishes and both characteristics reach a saturation-like level, where the volume specific surface area is close to the geometric maximum

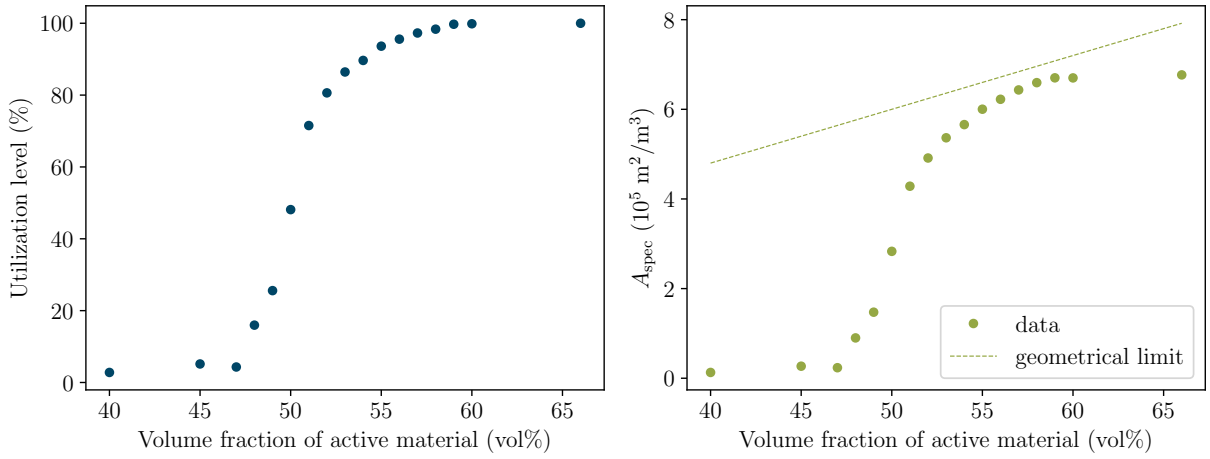

Figure 3: Utilization level of active material (left) and specific surface area of the electronic conduction cluster (right) at varying fraction of active material with 5 µm diameter. The geometrical limit (Equation 7) of the specific surface area is indicated by the dashed line.

$$A_{\mathrm{spec,geo}} = g^{\mathrm{V}}_{\mathrm{AM}} \frac{A_{\mathrm{sphere}}}{V_{\mathrm{sphere}}} = g^{\mathrm{V}}_{\mathrm{AM}} \frac{6}{d}, \tag{7}$$

and only few particles remain isolated.

To verify, whether the power law of percolation theory (Equation 1) is applicable for this kind of particle arrangements, the specific surface area just above the percolation threshold of the electronic cluster was calculated for a particle size of 10 µm, based on eight particle arrangements for each AM packing density. The data in the log-log plot in Figure 4 can indeed be fitted by a power law with a critical exponent of 0.41, even though the error bars, computed as the standard deviation, tend to become large in the vicinity of the transition. The particle size was arbitrarily chosen and we expect the power law to apply for any of the particle sizes studied in this work. The critical exponent of 0.41 is in good agreement with a study of 3D site-percolation in a simple cubic lattice performed by Sur et al.[37], indicating that the power law of percolation is applicable.

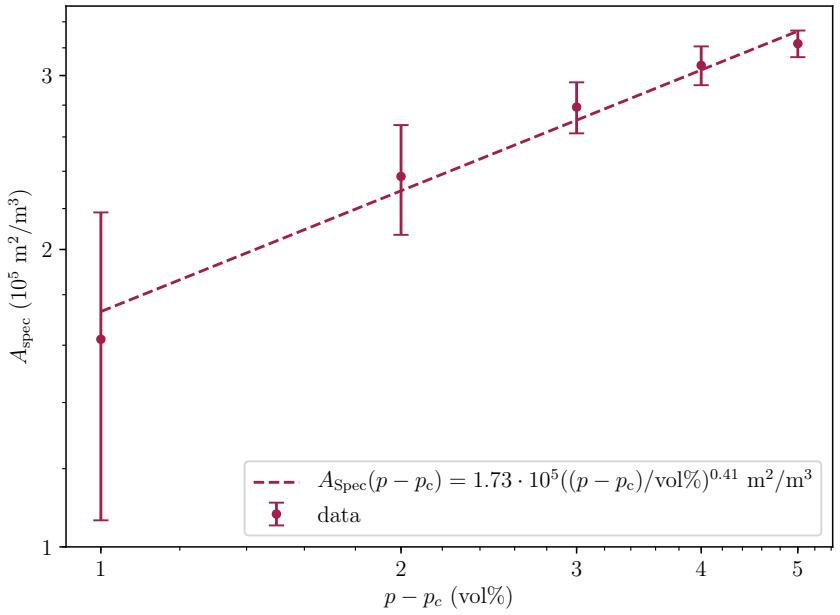

Figure 4: Specific surface area of the electronic cluster above percolation threshold for arbitrarily chosen AM particle size $d = 10$ µm featuring the power law predicted by percolation theory with a critical exponent of $\beta = 0.41$. The surface area is computed on the basis of eight particle arrangements for each packing density.

Model arrangements with particle sizes between 3 and 15 µm were built to compare the findings for 5 µm to other particle sizes. As before, one microstructure was computed for each AM fraction in sub- and super-critical regions and ten microstructures for each fraction in the transition region to avoid fluctuations. The utilization level and specific surface area for all different particle sizes are shown in Figure 5. As observed before (arrangements in Figure 2), smaller particles are in general more likely to develop percolation clusters at low AM fractions than larger particles. While the transition region of 3 µm particles is located within the interval of 41 to 46 vol%, it shifts towards higher fractions up to the interval of 52 to 57 vol% for 15 µm-sized particles. The steepness of the transition region is similar for all particle sizes. Here, the difference in the behaviors of utilization level and specific surface area can be observed: The smaller the particles, the higher the specific surface area gets. To quantify the effect of particle size, the percolation threshold is defined to be the AM volume fraction at which the majority of the ten arrangements features a percolating cluster. This corresponds to the AM volume fraction at which the mean utilization level is at 40 vol%. These thresholds with respect to the particle size are presented in Figure 6 and can be fitted

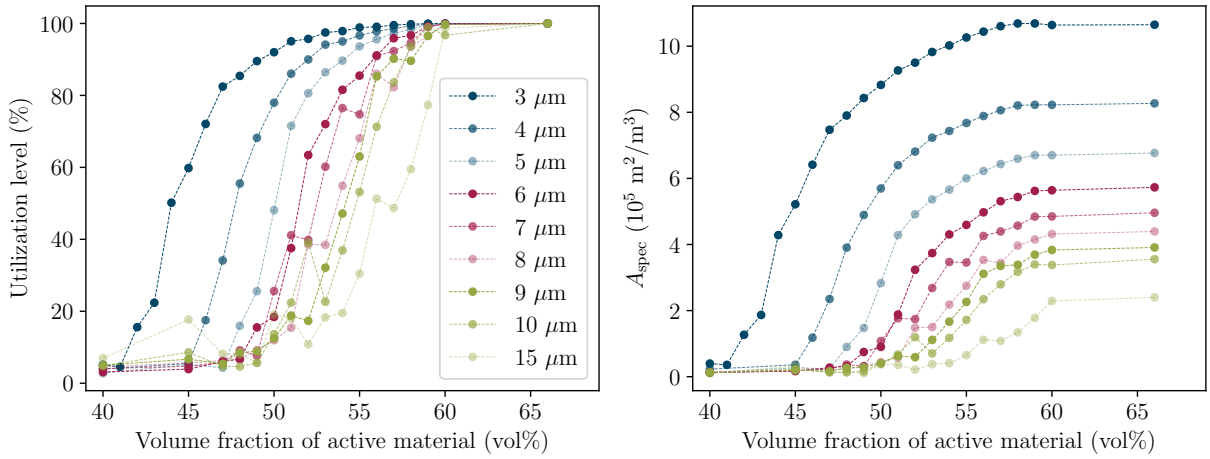

Figure 5: Utilization level of active material (left) and specific surface area of the electronic conduction cluster (right) at varying fraction of active material for various AM particle sizes between 3 and 15 µm.

by

$$p_c = [7.83 \ln(d/\mu m) + 36.67] \text{ vol\%}, \quad (8)$$

indicating a logarithmic relationship between AM particle size and percolation threshold. These findings correlate well with the observation of high fractions of inactive NCM-622 for large AM particle sizes, measured *via ex situ* X-Ray Diffraction (XRD) and with their attributed low effective electronic conductivity studied by Strauss et al.[13]. As large AM particles exhibit a smaller surface area, they offer less possibilities for percolating electronic clusters, and thus lead to lower effective electronic conductivity. Unfortunately, the total packing density of AM used by Strauss et al.[13] is not known, as the porosity was not measured.

Overall and according to the microstructural modeling, the effective electronic conduction within carbon-free composite cathodes is highly dependent on the packing density of the AM particles and on their size. Dense packing enables more intimate contact and higher

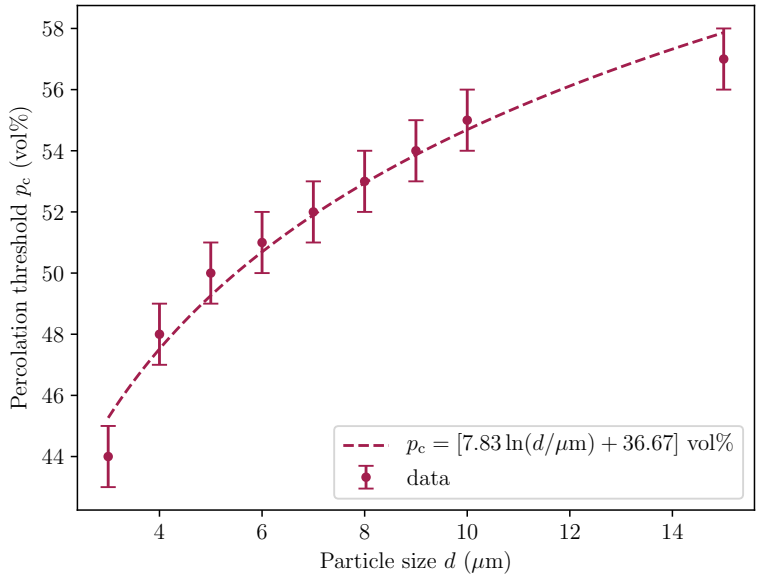

Figure 6: Dependence of the percolation threshold (in vol% of AM) of the electronic conduction cluster on AM particle size, fitted by a logarithmic function, which represents the data sufficiently accurate.

connectivity between AM particles, increases the fraction of active (connected) particles and therefore enhances electrode performance. Besides, small particles enable high utilization levels at lower packing density and might hence be a possibility to compensate for high porosities, even though the high surface area is vulnerable for chemical degradation and formation of passivating cathode/electrolyte interfacial layers upon charging[7], which may result in performance decrease.

Ionic Conduction

In addition to the electronically conducting microstructures, we will now take ionic conduction into account and examine its characteristics. Since small AM particles suggested good performance in the previous section and an AM particle diameter of 5 µm, according to Strauss et al.[13], is realistic for NCM-particles, this size is chosen for the calculation in this section. As the cathode composition and its porosity are not well-defined for a given total fraction of active material, two cases are distinguished: Constant porosity at varying composition and constant composition at varying porosity.

In the case of constant porosity, the composition (namely $g^{\mathrm{S}}_{\mathrm{AM}}/g^{\mathrm{S}}_{\mathrm{SE}}$) is calculated by

$$g^{\mathrm{S}}_{\mathrm{AM}} = \frac{g^{\mathrm{V}}_{\mathrm{AM}}}{1-\phi}, \tag{9}$$

the two sub-structures are merged and the conduction clusters are computed as described previously. As before, $g^{\mathrm{V}}_{\mathrm{AM}}$ is the AM fraction with respect to the total structure volume involving pore volume. It is also referred to as the total fraction of active material and has to be distinguished from the AM fraction in the solid phase $g^{\mathrm{S}}_{\mathrm{AM}}$, which does not include pore volume, but can be found directly in the composition indication.

For a porosity of 20 %, the resulting utilization levels of AM and SE, as well as the volume specific interface area, are shown in Figure 7. The presented utilization level reveals the limitations for cathode performance. While electronic conduction is the limiting factor

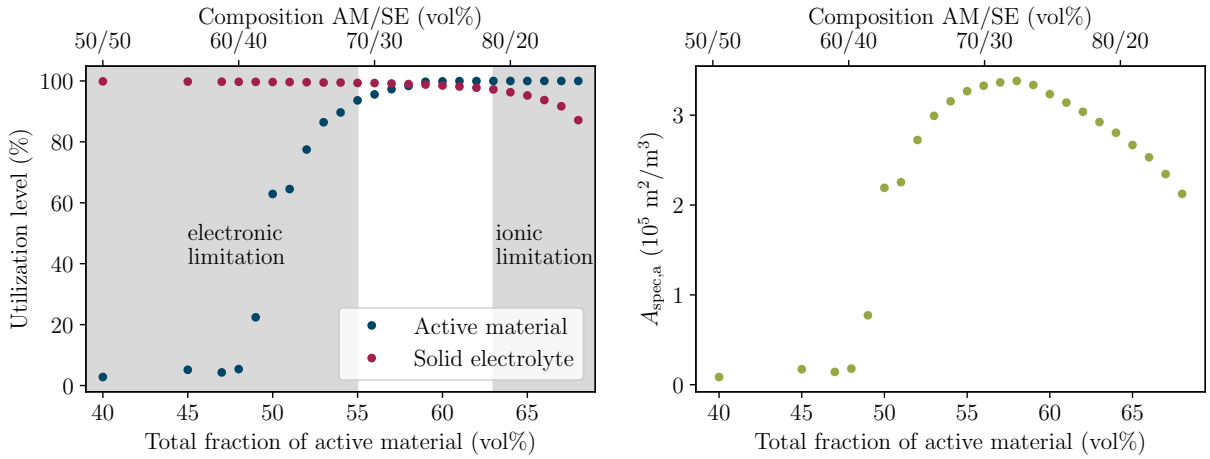

Figure 7: Utilization level of active material and solid electrolyte (left) and specific active interface area between the ionic and electronic conduction cluster (right) for composite cathode arrangements at a constant porosity of 20 % and AM particle size $d = 5$ µm. The lower x-axis reflects the total fraction of active material in the whole electrode, including porous space and solid electrolyte, while the composition shown in the upper x-axis reflects the AM and SE volume in the solid phase, only.

at compositions below 69 vol% active material and 31 vol% solid electrolyte (referred to as 69/31 vol%, subsequently), ionic conduction becomes restricting at high active material fractions and compositions above 79/21 vol%. Accordingly, the interval of well-performing composites is fairly small. Even though designed to overlap in the model, the solid electrolyte does not suffice to build well-connected ionic conduction clusters in highly AM-dominated microstructures. Correspondingly, the active interface area diminishes at higher active material fraction and an optimal composition can be identified at 72/28 vol% which corresponds to 86/14 wt% for NMC-622 and LPS.

In an analogous manner, the ideal composition can be modeled for other porosities, as demonstrated in Figure 8 for 5, 10 and 20 % porosity. As small porosities go along with high packing density and high mass loading, the active interfaces are significantly higher for 5 % porosity than for 10 or 20 %. Moreover, the electronic percolation transition takes place with smaller AM fractions than for more porous microstructures. Accordingly, an optimal composition is reached at 62/38 vol% (80/20 wt% for NMC-622 and LPS) for 5 %

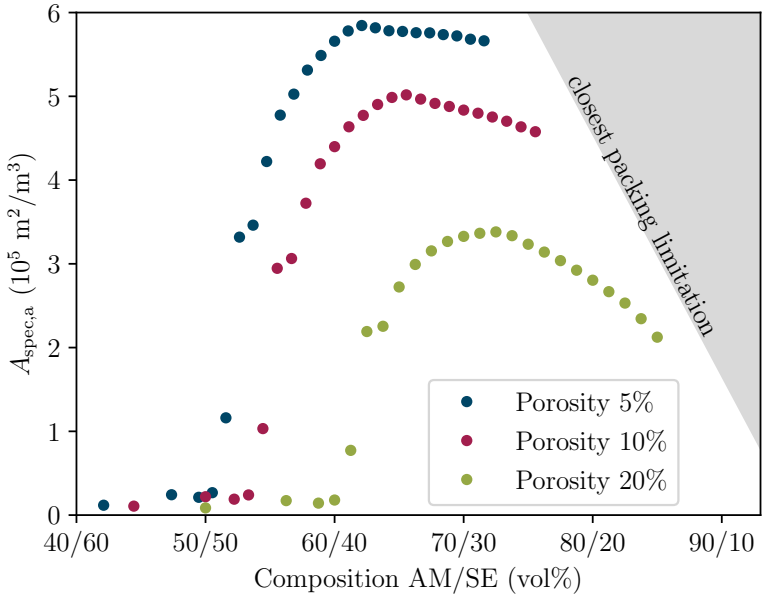

Figure 8: Specific active interface area between the ionic and electronic conduction cluster at different porosities for 5 µm-sized AM particles.

porosity, while 10 % porosity features an optimal composition of 66/34 vol% (82/18 wt% for NMC-622 and LPS). Apart from the shift of the optimal composition towards higher active material fractions for rising porosity, the ionic conduction limitation gains importance for higher porosities: The drop at compositions above the optimum is more pronounced at a porosity of 20 % compared to 5 and 10 %.

Keeping a constant composition and varying the porosity, the effect of densification of composite electrodes can be studied. Figure 9 shows the percolation properties for porosities from 43 % down to 3 % at a composition of 70/30 vol%. Evaluating the utilization of both materials, high porosities above 34 % are accompanied by ionically and electronically isolated regions in the cathode. The active interface is negligible in this section and increases for porosities below 30 %. Down to 21 % porosity, the electronic limitation is still present, but below this value, the cathodes ought to perform well. The behavior of the active interface area in Figure 9 is not as significant as in the case of constant porosity, because a lowering of porosity goes along with densification of the electrode, and thus more particles (both AM

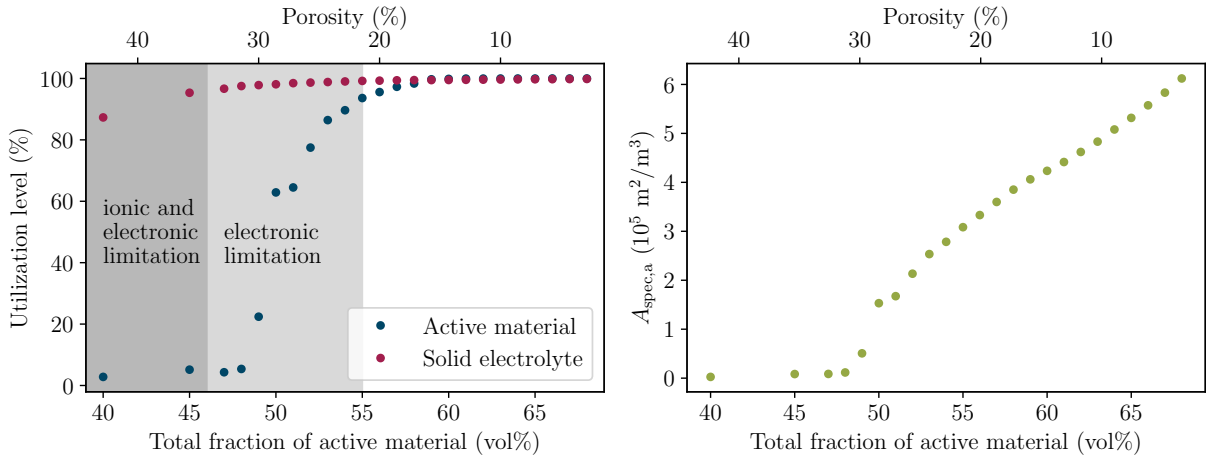

Figure 9: Porosity dependence of the utilization level of active material and solid electrolyte (left) and the specific active interface area between the ionic and electronic conduction cluster (right) for composite cathode microstructures at a constant composition of 70/30 vol% active material with electrolyte and AM particle size $d = 5$ µm. The lower x-axis reflects the total fraction of active material in the whole microstructure including porous space and solid electrolyte.

and SE) in the microstructure become connected, leading to higher surface areas. The reader may bear in mind that the active interface area is not normalized with respect to porosity, but with respect to the electrode volume.

Electrode thickness

Another key issue in composite electrode design for high energy batteries is the electrode thickness: How thick can an electrode get that performs well, even at higher C-rates[38,39]? Percolation represents one important aspect in the description of thick electrodes: Sufficient conduction networks are required, but diffusion lengths in the storage phase, tortuosity and resulting effective conductivities play an additional role in thick electrodes and are not explicitly treated in this study.

To analyze the effects of electrode thickness on ionic and electronic percolation, the initially created particle arrangements of 140 µm thickness were cut at different thicknesses between 20 and 120 µm. The associated active interface areas are shown in Figure 10 for

varying compositions at 20 % porosity. For most thicknesses, the active interface area is very similar throughout the whole composition range. The optimum is located at the same composition for all electrode arrangements studied, but the curve shape below the optimum differs, especially for thin electrodes. This is due to the electronic conduction cluster, whose starting point is located at the current collector side of the composite. In thin electrode microstructures, the initially connected particles take a higher fraction of the whole structure. Therefore, the specific active interface area is enhanced for thin electrodes even for low active material fractions. Furthermore, a slight shift in the percolation threshold can be observed: Thin composites tend to percolate at smaller AM fractions, even though the shift is not as distinct as it was for different particle sizes. As a result, percolation effects are suppressed in thin electrodes, giving the impression of favorable electrode properties. This is a direct effect of the reduced model size, also known as a finite size effect. The microstructures on the right of Figure 10 illustrate this phenomenon at an AM fraction of 47 vol% for an AM particle size of 5 µm. In contrast to the electronic conduction, ionic conduction is not affected by the electrode thickness: The drop of volume-specific active interface area (compare Figure 7) is indistinguishable for all thicknesses.

This shows that, solely judged by microstructural modeling, thick electrodes could provide conduction clustering properties comparable to those of thin electrodes. Even though the modeling technique does certainly not account for long diffusion paths and can therefore not directly reflect the charging and discharging performance, it is very efficient in identifying conduction clusters of composite cathodes based on particle size, shape and overlap properties.

The method has the potential to serve as a basis for studying composite electrode's behavior in more detail, incorporating the mathematical modeling of electrochemical reactions or the transformation of particle arrangements into resistor networks as performed by Sunde [40] and Ott et al. [41] for fuel cells.

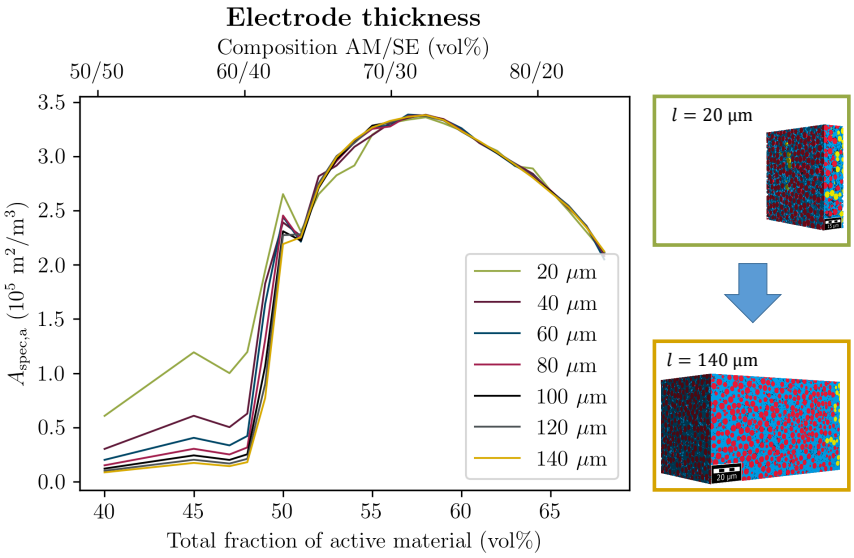

Figure 10: Specific interface area between the electronic and ionic cluster for different electrode thicknesses between 20 and 140 μm at a constant porosity of 20 % and an AM particle size of $d = 5$ μm. The lower x-axis reflects the total fraction of active material in the whole composite, including porous space and solid electrolyte, while the composition shown in the upper x-axis reflects the AM and SE volume in the solid phase, only. The microstructure models for minimal and maximal electrode thickness at 47 vol% AM fraction are shown (right).

Conclusions

We have established a microstructural modeling method with the aim to asses the electronic and ionic percolation behavior of composite cathodes for ASSBs. Consisting of active material and solid electrolyte, the resulting composite microstructures represent carbon-free solid-state cathodes, as experimentally corroborated by Strauss et al. [13]. Ionic and electronic conduction clusters have been calculated according to percolation theory and the resulting utilization levels and active interface areas were evaluated. Porosity, composition, electrode thickness and AM particle size were taken into account to collect information on how to design composite cathodes. We ultimately found that boundary conditions for well-connected cathodes can be defined.

In particular, small active material particles are desirable in terms of electronic conduction in carbon-free composites, since they offer higher active surface areas and more possibili-

ties to form percolating electronic clusters. Contrariwise, high active material surfaces may enhance degradation processes at the cathode electrolyte interface and therefore negatively influence cell performance[7].

Although not provided in many studies[5,7,11–15,17], the porosity has shown to be an important property for ASSB composite electrodes, that can crucially influence conduction clusters and therefore cell performance. Accordingly, we strongly propose for future experimental studies to take the impact of porosity into account. It is worthwhile to make the effort and measure or calculate this important characteristic for the sake of comparability between experimental studies. As expected, small porosities are favorable in terms of conduction clustering, which leads to the necessity of manufacturing low-porous electrodes as proposed by Kim et al.[42], who infiltrated a sulfide-based solid electrolyte into conventional LCO and graphite Li-ion battery electrodes, achieving calculated porosities around 6 to 8 % and demonstrating intimate ionic contacts.

Moreover, we have managed to identify ideal compositions that ensure both ionic and electronic conduction at given porosities, based on pure microstructural modeling, in which no material characteristics except for the particle's shape, size and overlap behavior have been used. Anyhow, the effective conductivity optimum may differ from the optimum in specific active interface area, especially for the electronic cluster, because therein the active material particles are designed to avoid overlap and, at low active material fraction, are mainly connected by point contacts leaving aside constriction resistances. At higher fractions, the overlap increases and the connection of the interfaces of the active material particles is improved.

In general, real solid-state battery cells are a time-variant system and the initial composition may change during cycling, incorporating particle cracks, volume changes and other mechanical or (electro-)chemical issues[43]. Active material coating, binder and conductive agent may influence the performance as well as inhomogenities in the electrode composition, which may arise due to processing conditions and lead to non-uniform current distribution that causes

even more difficulties. However, these issues are beyond the scope of this study, whose intent is to provide design guidelines and a performance estimation, forming a foundation for microstructural modeling of all-solid-state batteries which offers multiple possibilities to be expanded.

Acknowledgement

The authors thank the consortium of the "FELIZIA" project (03XO0026G), funded by the German Federal Ministry of Education and Research (BMBF) for fruitful discussions.

References

(1) Gallagher, K. G.; Trask, S. E.; Bauer, C.; Woehrle, T.; Lux, S. F.; Tschech, M.; Lamp, P.; Polzin, B. J.; Ha, S.; Long, B. et al. Optimizing Areal Capacities through Understanding the Limitations of Lithium-Ion Electrodes. *Journal of The Electrochemical Society* **2016**, *163*, A138–A149.

(2) Luntz, A. C.; Voss, J.; Reuter, K. Interfacial Challenges in Solid-State Li Ion Batteries. *J. Phys. Chem. Lett.* **2015**, *6*, 4599–4604.

(3) Zhang, Z.; Shao, Y.; Lotsch, B.; Hu, Y.-S.; Li, H.; Janek, J.; Nazar, L. F.; Nan, C.-W.; Maier, J.; Armand, M. et al. New Horizons for Inorganic Solid State Ion Conductors. *Energy Environ. Sci.* **2018**, *11*, 1945–1976.

(4) Janek, J.; Zeier, W. G. A Solid Future for Battery Development. *Nature Energy* **2016**, *1*, 16141.

(5) Kato, Y.; Hori, S.; Saito, T.; Suzuki, K.; Hirayama, M.; Mitsui, A.; Yonemura, M.; Iba, H.; Kanno, R. High-Power All-Solid-State Batteries using Sulfide Superionic Conductors. *Nature Energy* **2016**, *1*, 16030.

(6) Wu, B.; Wang, S.; Evans IV, W. J.; Deng, D. Z.; Yang, J.; Xiao, J. Interfacial Behaviours between Lithium Ion Conductors and Electrode Materials in Various Battery Systems. *J. Mater. Chem. A* **2016**, *4*, 15266–15280.

(7) Koerver, R.; Aygün, I.; Leichtweiß, T.; Dietrich, C.; Zhang, W.; Binder, J. O.; Hartmann, P.; Zeier, W. G.; Janek, J. Capacity Fade in Solid-State Batteries: Interphase Formation and Chemomechanical Processes in Nickel-Rich Layered Oxide Cathodes and Lithium Thiophosphate Solid Electrolytes. *Chemistry of Materials* **2017**, *29*, 5574–5582.

(8) Yamamoto, K.; Iriyama, Y.; Asaka, T.; Hirayama, T.; Fujita, H.; Fisher, C. A. J.; Nonaka, K.; Sugita, Y.; Ogumi, Z. Dynamic Visualization of the Electric Potential in an All-Solid-State Rechargeable Lithium Battery. *Angewandte Chemie International Edition* **2010**, *49*, 4414–4417.

(9) Raj, R.; Wolfenstine, J. Current Limit Diagrams for Dendrite Formation in Solid-State Electrolytes for Li-Ion Batteries. *Journal of Power Sources* **2017**, *343*, 119–126.

(10) Kerman, K.; Luntz, A.; Viswanathan, V.; Chiang, Y.-M.; Chen, Z. Review—Practical Challenges Hindering the Development of Solid State Li Ion Batteries. *Journal of The Electrochemical Society* **2017**, *164*, A1731–A1744.

(11) Nam, Y. J.; Oh, D. Y.; Jung, S. H.; Jung, Y. S. Toward Practical All-Solid-State Lithium-Ion Batteries with High Energy Density and Safety: Comparative Study for Electrodes Fabricated by Dry- and Slurry-Mixing Processes. *Journal of Power Sources* **2018**, *375*, 93–101.

(12) Zhang, W.; Weber, D. A.; Weigand, H.; Arlt, T.; Manke, I.; Schröder, D.; Koerver, R.; Leichtweiss, T.; Hartmann, P.; Zeier, W. G. et al. Interfacial Processes and Influence of Composite Cathode Microstructure Controlling the Performance of All-Solid-State Lithium Batteries. *ACS Applied Materials & Interfaces* **2017**, *9*, 17835–17845.

(13) Strauss, F.; Bartsch, T.; de Biasi, L.; Kim, A.-Y.; Janek, J.; Hartmann, P.; Brezesinski, T. Impact of Cathode Material Particle Size on the Capacity of Bulk-Type All-Solid-State Batteries. *ACS Energy Letters* **2018**, *3*, 992–996.

(14) Siroma, Z.; Sato, T.; Takeuchi, T.; Nagai, R.; Ota, A.; Ioroi, T. AC Impedance Analysis of Ionic and Electronic Conductivities in Electrode Mixture Layers for an All-Solid-State Lithium-Ion Battery. *Journal of Power Sources* **2016**, *316*, 215–223.

(15) Noh, S.; Nichols, W. T.; Park, C.; Shin, D. Enhanced Energy Density and Electrochemical Performance of All-Solid-State Lithium Batteries through Microstructural Distribution of Solid Electrolyte. *Ceramics International* **2017**, *43*, 15952–15958.

(16) Hlushkou, D.; Reising, A. E.; Kaiser, N.; Spannenberger, S.; Schlabach, S.; Kato, Y.; Roling, B.; Tallarek, U. The Influence of Void Space on Ion Transport in a Composite Cathode for All-Solid-State Batteries. *Journal of Power Sources* **2018**, *396*, 363–370.

(17) Kato, Y.; Shiotani, S.; Morita, K.; Suzuki, K.; Hirayama, M.; Kanno, R. All-Solid-State Batteries with Thick Electrode Configurations. *The Journal of Physical Chemistry Letters* **2018**, *9*, 607–613.

(18) Arora, P.; Doyle, M.; S. Gozdz, A.; E. White, R.; Newman, J. Comparison between Computer Simulations and Experimental Data for High-Rate Discharges of Plastic Lithium-Ion Batteries. **2000**, *88*, 219–231.

(19) Lagadec, M. F.; Zahn, R.; Müller, S.; Wood, V. Topological and Network Analysis of Lithium Ion Battery Components: The Importance of Pore Space Connectivity for Cell Operation. *ArXiv e-prints* **2018**, 1–8.

(20) Kesten, H. *Percolation Theory for Mathematicians*; Progress in probability and statistics; Birkhäuser, 1982; Vol. 2.

(21) Grimmett, G. In *Lectures on Probability Theory and Statistics: Ecole d'Eté de Probabilités de Saint-Flour XXVI-1996*; Bernard, P., Ed.; Springer Berlin Heidelberg: Berlin, Heidelberg, 1997; pp 153–300.

(22) Hoshen, J.; Kopelman, R. Percolation and Cluster Distribution. I. Cluster Multiple Labeling Technique and Critical Concentration Algorithm. *Phys. Rev. B* **1976**, *14*, 3438–3445.

(23) Zhang, W.; Leichtweiß, T.; Culver, S. P.; Koerver, R.; Das, D.; Weber, D. A.; Zeier, W. G.; Janek, J. The Detrimental Effects of Carbon Additives in $Li_{10}GeP_2S_{12}$-Based Solid-State Batteries. *ACS Applied Materials & Interfaces* **2017**, *9*, 35888–35896.

(24) Hakari, T.; Deguchi, M.; Mitsuhara, K.; Ohta, T.; Saito, K.; Orikasa, Y.; Uchimoto, Y.; Kowada, Y.; Hayashi, A.; Tatsumisago, M. Structural and Electronic-State Changes of a Sulfide Solid Electrolyte during the Li Deinsertion–Insertion Processes. *Chemistry of Materials* **2017**, *29*, 4768–4774.

(25) Ohta, N.; Takada, K.; Zhang, L.; Ma, R.; Osada, M.; Sasaki, T. Enhancement of the High-Rate Capability of Solid-State Lithium Batteries by Nanoscale Interfacial Modification. *Advanced Materials* **2006**, *18*, 2226–2229.

(26) Yada, C.; Lee, C. E.; Laughman, D.; Hannah, L.; Iba, H.; Hayden, B. E. A High-Throughput Approach Developing Lithium-Niobium-Tantalum Oxides as Electrolyte/Cathode Interlayers for High-Voltage All-Solid-State Lithium Batteries. *Journal of The Electrochemical Society* **2015**, *162*, A722–A726.

(27) Ohta, N.; Takada, K.; Sakaguchi, I.; Zhang, L.; Ma, R.; Fukuda, K.; Osada, M.; Sasaki, T. $LiNbO_3$-Coated $LiCoO_2$ as Cathode Material for All Solid-State Lithium Secondary Batteries. *Electrochemistry Communications* **2007**, *9*, 1486–1490.

(28) Ohtomo, T.; Hayashi, A.; Tatsumisago, M.; Tsuchida, Y.; Hama, S.; Kawamoto, K. All-Solid-State Lithium Secondary Batteries using the $75Li_2S{\cdot}25P_2S_5$ Glass and the

$70Li_2S{\cdot}30P_2S_5$ Glass–Ceramic as Solid Electrolytes. *Journal of Power Sources* **2013**, *233*, 231–235.

(29) Ito, S.; Fujiki, S.; Yamada, T.; Aihara, Y.; Park, Y.; Kim, T. Y.; Baek, S.-W.; Lee, J.-M.; Doo, S.; Machida, N. A Rocking Chair Type All-Solid-State Lithium Ion Battery Adopting Li_2O–ZrO_2 Coated $LiNi_{0.8}Co_{0.15}Al_{0.05}O_2$ and a Sulfide Based Electrolyte. *Journal of Power Sources* **2014**, *248*, 943–950.

(30) Math2Market GmbH, K. G. GeoDict – The Digital Material Laboratory, Version 2018 SP 5. 2018.

(31) Tóth, L. F. *Dichteste Kugelpackung. Eine Idee von Gauß*; Abhandlungen der Braunschweigischen Wissenschaftlichen Gesellschaft; Goltze: Göttingen, 1977; Vol. 27.

(32) Sakuda, A.; Hayashi, A.; Tatsumisago, M. Sulfide Solid Electrolyte with Favorable Mechanical Property for All-Solid-State Lithium Battery. *Scientific Reports* **2013**, *3*.

(33) Yang, Y.; Wu, Q.; Cui, Y.; Chen, Y.; Shi, S.; Wang, R.-Z.; Yan, H. Elastic Properties, Defect Thermodynamics, Electrochemical Window, Phase Stability, and Li^+ Mobility of Li_3PS_4: Insights from First-Principles Calculations. *ACS Applied Materials & Interfaces* **2016**, *8*, 25229–25242.

(34) Deng, Z.; Wang, Z.; Chu, I.-H.; Luo, J.; Ong, S. Elastic Properties of Alkali Superionic Conductor Electrolytes from First Principles Calculations. *Journal of The Electrochemical Society* **2016**, *163*, A67–A74.

(35) Amin, R.; Chiang, Y.-M. Characterization of Electronic and Ionic Transport in $Li_{1-x}Ni_{0.33}Mn_{0.33}Co_{0.33}O_2$ (NMC333) and $Li_{1-x}Ni_{0.50}Mn_{0.20}Co_{0.30}O_2$ (NMC523) as a Function of Li Content. *Journal of The Electrochemical Society* **2016**, *163*, A1512–A1517.

(36) Greenwood, J. A. Constriction Resistance and the Real Area of Contact. *British Journal of Applied Physics* **1966**, *17*, 1621.

(37) Sur, A.; Lebowitz, J. L.; Marro, J.; Kalos, M. H.; Kirkpatrick, S. Monte Carlo Studies of Percolation Phenomena for a Simple Cubic Lattice. *Journal of Statistical Physics* **1976**, *15*, 345–353.

(38) Singh, M.; Kaiser, J.; Hahn, H. Thick Electrodes for High Energy Lithium Ion Batteries. *Journal of The Electrochemical Society* **2015**, *162*, A1196–A1201.

(39) Danner, T.; Singh, M.; Hein, S.; Kaiser, J.; Hahn, H.; Latz, A. Thick Electrodes for Li-Ion Batteries: A Model Based Analysis. *Journal of Power Sources* **2016**, *334*, 191–201.

(40) Sunde, S. Simulations of Composite Electrodes in Fuel Cells. *Journal of Electroceramics* **2000**, *5*, 153–182.

(41) Ott, J.; Völker, B.; Gan, Y.; McMeeking, R. M.; Kamlah, M. A Micromechanical Model for Effective Conductivity in Granular Electrode Structures. *Acta Mechanica Sinica* **2013**, *29*, 682–698.

(42) Kim, D. H.; Oh, D. Y.; Park, K. H.; Choi, Y. E.; Nam, Y. J.; Lee, H. A.; Lee, S.-M.; Jung, Y. S. Infiltration of Solution-Processable Solid Electrolytes into Conventional Li-Ion-Battery Electrodes for All-Solid-State Li-Ion Batteries. *Nano Letters* **2017**, *17*, 3013–3020.

(43) Koerver, R.; Zhang, W.; de Biasi, L.; Schweidler, S.; Kondrakov, A. O.; Kolling, S.; Brezesinski, T.; Hartmann, P.; Zeier, W. G.; Janek, J. Chemo-Mechanical Expansion of Lithium Electrode Materials - On the Route to Mechanically Optimized All-Solid-State Batteries. *Energy Environ. Sci.* **2018**, *11*, 2142–2158.

TOC Graphic

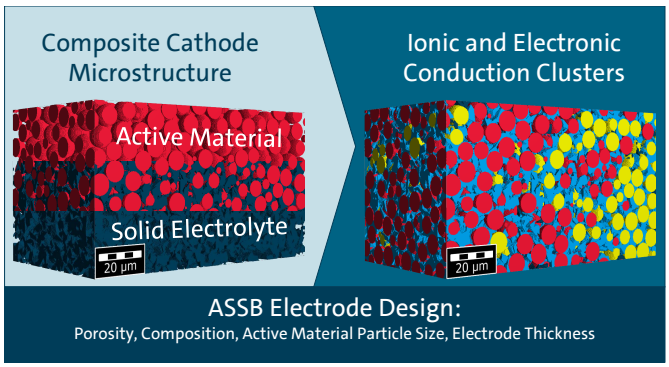
Composite Cathode Microstructure
Active Material
Solid Electrolyte
20 µm
Ionic and Electronic Conduction Clusters
20 µm
ASSB Electrode Design:
Porosity, Composition, Active Material Particle Size, Electrode Thickness